The Astrophysical Journal Letters, 973:L30 (8pp), 2024 September 20 https://doi.org/10.3847/2041-8213/ad77d9


# TESS Investigation—Demographics of Young Exoplanets (TI-DYE). II. A Second Giant Planet in the 17 Myr System HIP 67522

Madyson G. Barber[1,16], Pa Chia Thao[1,16,17], Andrew W. Mann[1], Andrew Vanderburg[2], Mayuko Mori[3,4], John H. Livingston[3,4,5], Akihiko Fukui[6,7], Norio Narita[3,6,7], Adam L. Kraus[8], Benjamin M. Tofflemire[8,18], Elisabeth R. Newton[9], Joshua N. Winn[10], Jon M. Jenkins[11], Sara Seager[2,12,13], Karen A. Collins[14], and Joseph D. Twicken[11,15]

[1] Department of Physics and Astronomy, The University of North Carolina at Chapel Hill, Chapel Hill, NC 27599, USA; madysonb@live.unc.edu
[2] Department of Physics and Kavli Institute for Astrophysics and Space Research, Massachusetts Institute of Technology, Cambridge, MA 02139, USA
[3] Astrobiology Center, 2-21-1 Osawa, Mitaka, Tokyo 181-8588, Japan
[4] National Astronomical Observatory of Japan, 2-21-1 Osawa, Mitaka, Tokyo 181-8588, Japan
[5] Department of Astronomy, School of Science, The Graduate University for Advanced Studies (SOKENDAI), 2-21-1 Osawa, Mitaka, Tokyo, Japan
[6] Komaba Institute for Science, The University of Tokyo, 3-8-1 Komaba, Meguro, Tokyo 153-8902, Japan
[7] Instituto de Astrofísica de Canarias (IAC), 38205 La Laguna, Tenerife, Spain
[8] Department of Astronomy, The University of Texas at Austin, Austin, TX 78712, USA
[9] Department of Physics and Astronomy, Dartmouth College, Hanover, NH 03755, USA
[10] Department of Astrophysical Sciences, Princeton University, 4 Ivy Lane, Princeton, NJ 08544, USA
[11] NASA Ames Research Center, Moffett Field, CA, 94035, USA
[12] Department of Earth, Atmospheric and Planetary Sciences, Massachusetts Institute of Technology, Cambridge, MA 02139, USA
[13] Department of Aeronautics and Astronautics, MIT, 77 Massachusetts Avenue, Cambridge, MA 02139, USA
[14] Center for Astrophysics | Harvard & Smithsonian, 60 Garden Street, Cambridge, MA 02138, USA
[15] SETI Institute, Mountain View, CA 94043, USA
*Received 2024 July 5; revised 2024 August 13; accepted 2024 August 21; published 2024 September 19*

## Abstract

The youngest (<50 Myr) planets are vital to understand planet formation and early evolution. The 17 Myr system HIP 67522 is already known to host a giant ($\simeq 10 R_\oplus$) planet on a tight orbit. In their discovery paper, Rizzuto et al. reported a tentative single-transit detection of an additional planet in the system using TESS. Here, we report the discovery of HIP 67522c, a 7.9 $R_\oplus$ planet that matches with that single-transit event. We confirm the signal with ground-based multiwavelength photometry from Sinistro and MuSCAT4. At a period of 14.33 days, planet c is close to a 2:1 mean-motion resonance with b (6.96 days or 2.06:1). The light curve shows distortions during many of the transits, which are consistent with spot-crossing events and/or flares. Fewer stellar activity events are seen in the transits of planet b, suggesting that planet c is crossing a more active latitude. Such distortions, combined with systematics in the TESS light-curve extraction, likely explain why planet c was previously missed.

*Unified Astronomy Thesaurus concepts:* Exoplanets (498); Transit photometry (1709); Stellar activity (1580); Exoplanet evolution (491); Young stellar objects (1834)

*Materials only available in the online version of record: data behind figures*

## 1. Introduction

Young (<500 Myr) planets provide an opportunity to detect planet-sculpting processes as they happen. In particular, young multiplanet systems are valuable because they allow for better control of variables within a single system and enable a wider range of science cases than those with single planets. Such systems enable tests on the origin of intrasystem uniformity (e.g., J. J. Lissauer et al. 2011; C. Lammers et al. 2023), differential measurements of planetary atmospheres within a system (comparative planetology; e.g., S. Barat et al. 2024), and searches for transit timing variations (TTVs) that may yield precise masses and eccentricities (e.g., J. H. Steffen et al. 2012; K. Masuda 2014), among a wide range of other science cases.

Stellar, and hence planetary, ages are generally challenging to determine for individual systems (D. R. Soderblom et al. 2014). Therefore, planets in stellar associations are critical to understanding planet formation mechanisms, as the planets' ages can be precisely derived from the parent stellar population. Studies from the small sample of young planets (<30) have demonstrated several key findings: some close-in planets either form in situ or migrate quickly (T. J. David et al. 2019a; A. W. Mann et al. 2022; M. L. Wood et al. 2023), young planets tend to be larger than their older counterparts (R. B. Fernandes et al. 2022, 2023; S. Vach et al. 2024a), and among the six <100 Myr planets with Rossiter–McLaughlin or Doppler tomography, all are aligned or nearly aligned (e.g., T. Hirano et al. 2020; M. C. Johnson et al. 2022; T. Hirano et al. 2024).

TESS (G. R. Ricker et al. 2015) and *K*2 (S. B. Howell et al. 2014) have played critical roles in the discovery and characterization of young planetary systems. Light curves from these missions have been used to discover systems as young as 11 Myr (A. W. Mann et al. 2022; O. V. Zakhozhay et al. 2022) and young planets as small as $\simeq 1 R_\oplus$ (J. H. Livingston et al. 2018; B. K. Capistrant et al. 2024), as well as aid in the

[16] NSF Graduate Research Fellow.
[17] Jack Kent Cooke Foundation Graduate Scholar.
[18] 51 Pegasi b Fellow.

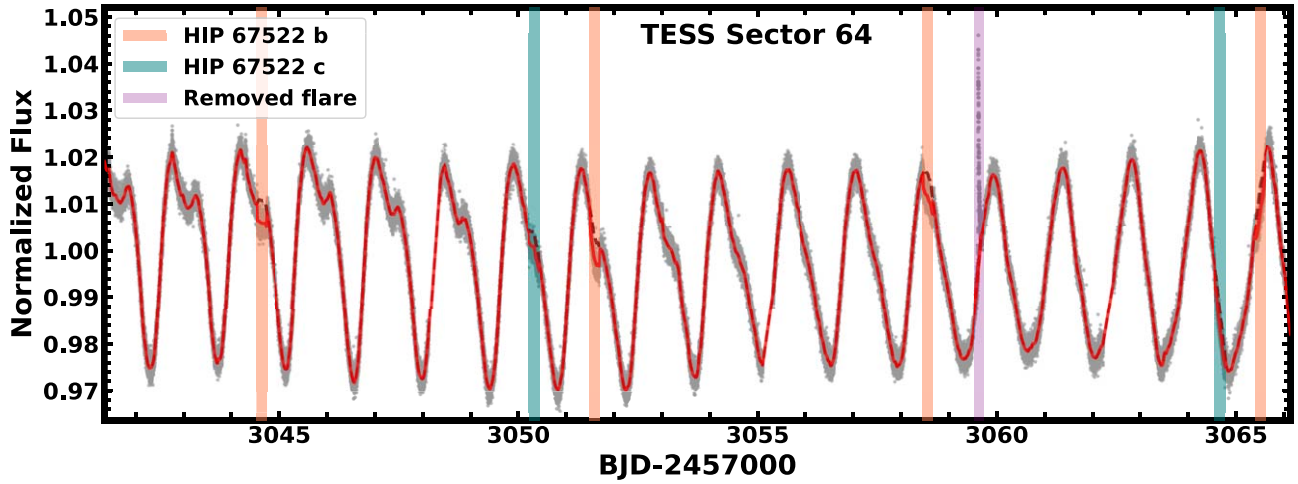


**Figure 1.** Representative section of the TESS light curve (gray points) with the best-fit GP model (red line). The locations of transits of HIP 67522b and c and the location of the removed flare are shown as the highlighted regions. The data set used to create this figure is available for download from the online journal.
(The data used to create this figure are available in the online article.)

discovery of new young stellar associations hosting transiting planets (e.g., B. M. Tofflemire et al. 2021; D. Nardiello et al. 2022; P. C. Thao et al. 2024).

One such important discovery is the young, hot, 10 $R_\oplus$ HIP 67522b (A. C. Rizzuto et al. 2020). The planet was identified using the `Notch` & `LoCoR` pipeline (`N&L`; A. C. Rizzuto et al. 2017) and TESS photometry. At 17 Myr, HIP 67522b stands as one of the youngest transiting planets known. It orbits a bright ($V = 9.8$) G-star in the nearby Scorpius-Centaurus OB association, which made it a prime target for transmission spectroscopy with JWST (A. W. Mann et al. 2021), Rossiter–McLaughlin observations (A. Heitzmann et al. 2021), and studies of atmospheric escape (R. P. Milburn et al. 2024, in preparation).

A. C. Rizzuto et al. (2020) noted a single trapezoid-like event in the light curve, consistent with an additional transiting planet (HIP 67522c). However, they detected no additional transit-like signals and hence could not confirm the signal as planetary in origin. Lacking evidence of another transit, it was assumed the candidate planet had a period >24 days (based on the time from the transit to the end of the sector). Based on the observed transit duration, the estimated orbital period was between 30 and 124 days (with 68% confidence).

Since the discovery, TESS reobserved the HIP 67522 system in two more sectors, and many teams have made improvements in the handling of TESS light curves for young stars (e.g., B. K. Capistrant et al. 2024). Using these data and our updated pipeline, we recover the original candidate transit alongside four other consistent transit-like events, yielding a period of 14.33 days (henceforth HIP 67522c). This places HIP 67522c close to the 2:1 resonance with HIP 67522b. The planet's large size, proximity to a mean-motion resonance (MMR), and age make it a compelling target for additional follow-up.

## 2. TESS Light Curve

HIP 67522 (TIC 166527623; TOI-6551; HD 120411) was first observed by TESS in Sector 11, from 2019 April 23 to 2019 May 20, and was reobserved in Sector 38 (2021 April 29–2021 May 26) and Sector 64 (2023 April 6–2023 May 3). The target was preselected for 2 minute short-cadence light curves for Sector 11 (G011280, PI A. Rizzuto) and Sector 38 (G03141, PI E. Newton and G03130, PI A. Mann) and 20 s light curves for Sector 64 (G05015, PI B. Hord and G05106, PI E. Gillen). In total, TESS observed five transits of HIP 67522c.

### 2.1. Extraction Pipeline

For our analysis, we used a custom light-curve extraction pipeline starting from simple aperture photometry (SAP; J. D. Twicken et al. 2010; R. L. Morris et al. 2020) fluxes from the Science Processing Operations Center (SPOC; J. M. Jenkins et al. 2016). We used the shortest-cadence data available for each sector. All TESS light curves used in this analysis can be found in MAST: 10.17909/9deq-2151.

We applied systematic corrections following the prescription in A. Vanderburg et al. (2019). To summarize, we corrected the SPOC SAP light curves with a linear model consisting of a basis spline (B-spline) with regularly spaced breaks at 0.2 day intervals to model long-term, low-frequency stellar variability, several moments of the distribution of the spacecraft quaternion time series measurements within each exposure, seven cotrending basis vectors from the SPOC Presearch Data Conditioning (PDC; J. C. Smith et al. 2012; M. C. Stumpe et al. 2012, 2014) band-3 flux time series correction with the largest eigenvalues, and a high-pass (0.1 day) time series from the SPOC background aperture. A representative section of the light curve can be seen in Figure 1. Additional details required to reproduce this correction can be found in A. Vanderburg et al. (2019).

We estimated the uncertainties on the flux by taking the median value of three different methods: (1) the median absolute deviation of the point minus the adjacent point; (2) the mean absolute deviation of the flattened light curve (flattened using `lightkurve`; Lightkurve Collaboration et al. 2018, with a 4$\sigma$ outlier threshold); and (3) sigma clipping, applying a median filter, sigma clipping again, and fitting a Gaussian to the resulting distribution of points. Each method was broadly consistent with each other, and the final results do not depend on the uncertainty estimate. We found the uncertainties for each sector separately and adopted an uncertainty of 0.0007, 0.0009, and 0.0014 for Sectors 11, 38, and 64, respectively.

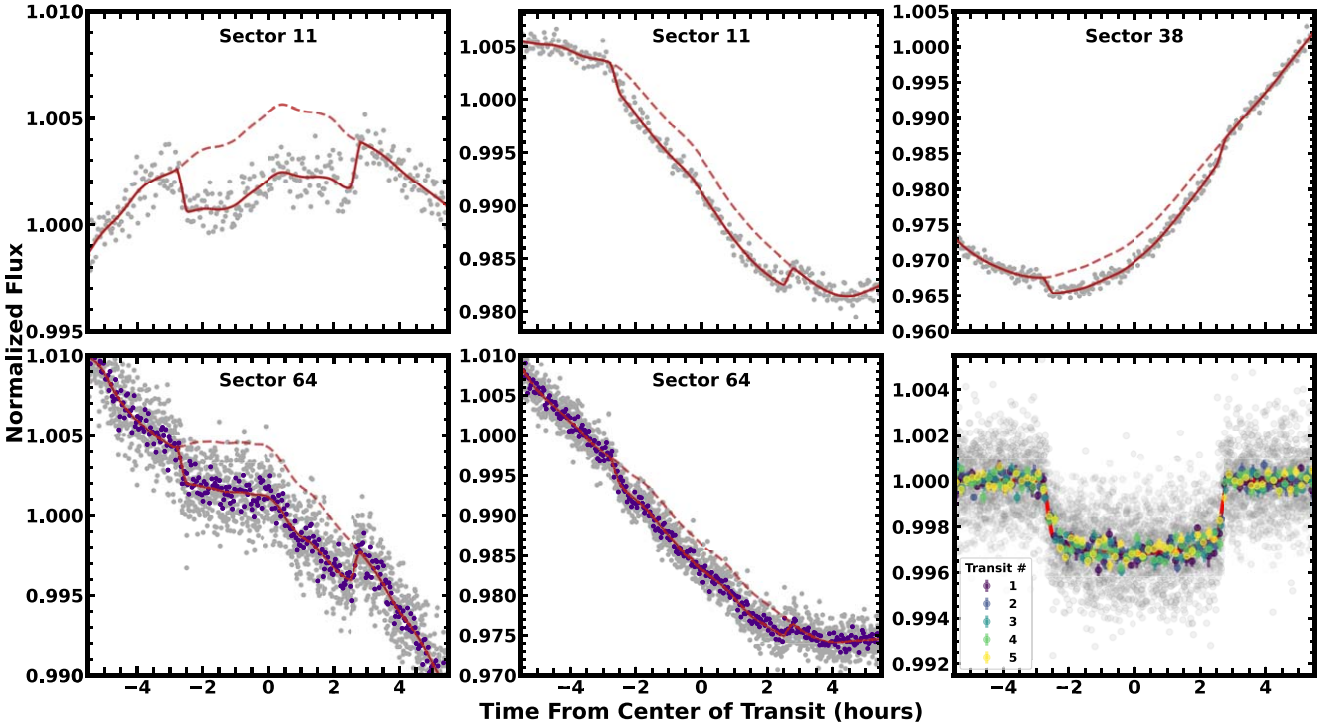


**Figure 2.** Individual transits of HIP 67522c and the GP model. Data in Sector 64 (20 s cadence) are binned to 2 minute intervals for easier comparison with Sector 11 and 38 (2 minute cadence). The transits show high levels of in-transit variation (potentially due to spot crossings). Bottom right: phase-folded light curve of HIP 67522 taken with TESS (gray points) and individual transits binned to 10 minute intervals (colored points) after the GP model of stellar variability has been removed. The best-fit model transit of HIP 67522c is shown as the red line. The data set used to create this figure is available for download from Figure 1 in the online journal.

## 3. Identification of the Transit

As part of our search for transiting planets in the youngest stellar associations (M. G. Barber et al. 2024, in preparation), and motivated by both the single-transit detection in A. C. Rizzuto et al. (2020) and the recent TTVs detected in HIP 67522b (P. C. Thao et al. 2024, in preparation), we searched HIP 67522 for additional planet signals. We used the updated `N&L` pipeline (A. C. Rizzuto et al. 2017)[19] as described in M. G. Barber et al. (2024, in preparation). To summarize, we updated the default box least-squares (BLS) search to the more recent implementation in `astropy`[20] (version 4.2; Astropy Collaboration et al. 2018) and used a more optimized period and duration search grid.

Using `Notch`, we detrended the light curve using a 0.3 day filtering window, which removes the stellar variability using a second-order polynomial while preserving the trapezoidal, transit-like signals. We then searched for repeated signals between 0.5 and 30 days with a signal-to-noise ratio (SNR) >8 using the BLS. We recovered the 6.9 day signal (HIP 67522b) at a BLS SNR of 29 and a 14.3 day signal with a BLS SNR of 17 (HIP 67522c).

Multiple transit signals of HIP 67522c are visible by eye in both the PDC SAP and systematics-corrected light curves before detrending. However, the original implementation of the `N&L` BLS did not recover the second planet signal, nor was it detected when using the PDC SAP flux (independent of the BLS implementation). In addition, using the default SPOC SAP or PDS SAP flux yielded transits with inconsistent depths over the full TESS curve. We only recovered the planet when using the updated light curves *and* the updated BLS implementation and only obtained a consistent transit signal when using the updated light curves.

Many of the HIP 67522c transits in the TESS light curve show evidence of local flares or spot crossings (see Figure 2). The second transit in the Sector 11 data contains such an event during midtransit, causing an irregular transit shape. These distortions are likely a major contributor to the fact that the planet was not recovered in prior searches.

The TESS SPOC search also recovered a signal from HIP 67522c in a multisector search of sectors 11, 38, and 64 conducted on 2023 June 21 with a noise-compensating matched filter (J. M. Jenkins et al. 2020), although at a significantly lower SNR than the notch-based detection. This elevated the detection to a threshold-crossing event, but it failed the ghost diagnostic test and was never elevated to a TESS object of interest (TOI).

## 4. Ground-based Follow-up

### 4.1. MuSCAT4

On 2024 April 22, we observed a predicted transit of HIP 67522c using the Multicolor Simultaneous Camera for studying Atmospheres of Transiting exoplanets (MuSCAT4; N. Narita et al. 2020) on the 2 m Faulkes Telescope South of Las Cumbres Observatory (LCO) at the Siding Spring Observatory in Australia. MuSCAT4 has a field of view of $9\farcm1 \times 9\farcm1$ and a pixel scale of $0\farcs27$ pixel$^{-1}$. With MuSCAT4, we simultaneously imaged HIP 67522 in the $g'$, $r'$, $i'$, and $z_s$ bands with exposure times of 12, 7, 8, and 5 s, respectively. Due to poor weather, we were unable to observe the transit egress.

We extracted the light curves using the standard LCOGT BANZAI pipeline (C. McCully et al. 2018) and applying a

[19] https://github.com/arizzuto/Notch_and_LOCoR
[20] http://www.astropy.org

customized aperture photometry pipeline for MuSCAT data (A. Fukui et al. 2011). We chose an optimal aperture radius and a set of comparison stars for each band that minimized the dispersion of the light curve.

### 4.2. Sinistro

We observed a predicted transit of HIP 67522c on 2024 May 6 simultaneously using three LCO 1 m telescopes with the Sinistro cameras. For all observations we used the $r'$ filter and an exposure time of 10 s.

All the images were calibrated using the standard LCOGT BANZAI pipeline. For two of the three data sets, we performed aperture photometry with `Photutils` and eight comparison stars. For the other data set, we applied aperture photometry using the same pipeline as used for the MuSCAT4 data. The differences between these extractions were minor, and the resulting three light curves were consistent with each other, so we combined them after applying a small y-offset to ensure the median values matched (a 0.02% correction).

## 5. Stellar Properties

A. C. Rizzuto et al. (2020) estimated the stellar radius ($R_* = 1.38 \pm 0.06 R_\odot$), effective temperature ($T_{\rm eff} = 5675 \pm 75$ K), and luminosity ($L_* = 1.75 \pm 0.09 L_\odot$) of HIP 67522 by fitting the spectral energy distribution (SED) with a grid of templates. They estimated the stellar mass ($M_*$) and age by interpolating the observed properties onto the PARSECv1.2S (A. Bressan et al. 2012) and BHAC15 (I. Baraffe et al. 2015) stellar evolutionary models.

Since the discovery, there have been new analyses of the Sco-Cen region that may impact these results. S. Ratzenböck et al. (2023) found the host star was in the $\nu$-Cen group, to which they assign an age between 9.5 and 15.7 Myr depending on the model and input photometry, consistent with the A. C. Rizzuto et al. (2020) estimate ($17 \pm 2$ Myr). R. Kerr et al. (2021) placed HIP 67522 in the "unclustered" region of Upper Centarus Lupus and were unable to assign a more precise age.

We also repeated the analysis from A. C. Rizzuto et al. (2020) using the Gaia DR3 parallax and photometry (Gaia Collaboration et al. 2023). All parameters were within $1\sigma$ of the values from A. C. Rizzuto et al. (2020). Because these and the above age determinations would result in negligible changes, we opted to keep the stellar parameters from A. C. Rizzuto et al. (2020) for all analyses.

## 6. Planet Properties

### 6.1. TESS Transit Fit

We fit the systematics-corrected TESS using `MISTTBORN` (MCMC Interface for Synthesis of Transits, Tomography, Binaries, and Others of a Relevant Nature; A. W. Mann et al. 2016; M. C. Johnson et al. 2018), which uses `BATMAN` to generate model transits (L. Kreidberg 2015), `celerite` to model stellar variability with a Gaussian process (GP; D. Foreman-Mackey et al. 2017), and `emcee` to explore the parameter space (D. Foreman-Mackey et al. 2013). Prior to fitting, we manually removed a large flare from 2460059.595 to 2460059.7 BJD.

We fit both planets b and c and the stellar variability simultaneously, with 19 fit parameters in total. For each planet, we fit for the time of periastron ($T_0$), planet orbital period ($P$), planet-to-star radius ratio ($R_p/R_*$), impact parameter ($b$), and $\sqrt{e}\cos\omega$ and $\sqrt{e}\sin\omega$ to account for orbital eccentricity ($e$) and the argument of periastron ($\omega$). We fit both planets with a common stellar density ($\rho_*$) and quadratic limb-darkening coefficients following triangular sampling ($q_1$, $q_2$; D. M. Kipping 2013).

The remaining four parameters were used to fit for the stellar variability in the GP model. We used a stochastically driven damped simple harmonic oscillator, following E. A. Gilbert et al. (2022), with a jitter term. The free parameters were the undampened oscillator period ($P$), the standard deviation of the process ($\sigma$), the damping timescale ($\tau$), and the jitter term ($\ln f$). This is a modified version of the `RotationTerm` in `Celerite2` (D. Foreman-Mackey 2018).

Most parameters evolved under uniform priors with only physical limitations. The TTV amplitude is small (<10 minutes), with the TESS data alone being consistent with a linear ephemeris (P. C Thao et al. 2024, in preparation), and did not impact our results. For $\rho_*$, we used a Gaussian prior from the SED and isochrone fits reported in A. C. Rizzuto et al. (2020), $\rho_*/\rho_\odot = 0.46 \pm 0.06$. With this prior on $\rho_*$, the transits primarily constrain eccentricity and $\omega$, instead of $\rho_*$ (see R. I. Dawson & J. A. Johnson 2012; V. Van Eylen & S. Albrecht 2015). We applied a Gaussian prior on the limb-darkening coefficients ($0.425 \pm 0.07$ and $0.153 \pm 0.05$) derived using the `LDTK` toolkit (H. Parviainen & S. Aigrain 2015) and our adopted stellar parameters.

We ran Markov Chain Monte Carlo (MCMC) using 50 walkers for 250,000 steps including a 50,000-step burn in. The total run was more than 50 times the autocorrelation time, indicating the number of steps was sufficient for convergence. We present the best-fit parameters in Table 1 and the phase-folded light curve for HIP 67522c in Figure 2. We also show a section of the TESS light curve with the GP model and locations of transits of both planets in Figure 1.

### 6.2. Ground-based Transit Fits

Our primary goal for the ground-based data was to confirm the transit depth is consistent with wavelength. To this end, we used an MCMC framework with the `BATMAN` (L. Kreidberg 2015) transit model. Each fit included a total of 16 parameters.

In the MuSCAT4 data, there is a perturbation between 2460422.985 and 2460423.05 BJD. Similarly, in the Sinistro simultaneous $r'$ transits, all three data sets exhibit a small spike in flux around 2460437.445 BJD. As we discuss further in Section 8, these were most likely spot crossings and were also seen in the TESS data. Some events may be flares (particularly the first bump in the MuSCAT4 data); however, our Gaussian spot model (below) described the deviations well.

To model the spot crossings, we used a Gaussian function, following F. Dai et al. (2017). For each spot, we fit for the spot timing ($t_{\rm sp}$), the spot amplitude ($A$), and the spot duration ($\tau$):

$$\mathrm{Spot}(t) = A \times \exp\left[\frac{-(t - t_{\rm sp})^2}{2\tau^2}\right]. \quad (1)$$

We handled the out-of-transit variability using a second-order polynomial, expressed as

$$\mathrm{flux}_{\rm corrected} = \mathrm{flux}_{\rm raw} \times (a + b \times t + c \times t^2). \quad (2)$$

We use an additional free parameter ($\ln f$) to capture any underestimated uncertainties. The $f$ parameter is an additional

**Table 1**
Parameters of the HIP 67522 System from TESS

| Parameter | Value | |
|---|---|---|
| | Stellar Parameters | |
| $\rho_\star$ ($\rho_\odot$) | $0.446^{+0.054}_{-0.047}$ | |
| $q_{1,1}$ | $0.153^{+0.049}_{-0.048}$ | |
| $q_{2,1}$ | $0.354^{+0.038}_{-0.040}$ | |
| | GP Parameters | |
| $P$ (days) | $1.177^{+0.033}_{-0.029}$ | |
| $\sigma$ | $0.0248^{+0.0013}_{-0.0011}$ | |
| $\tau$ (days) | $1.204^{+0.045}_{-0.037}$ | |
| $\ln f$ | $-13.2^{+1.3}_{-1.2}$ | |
| Parameter | $b$ | $c$ |
| | Measured Planet Parameters | |
| $T_0$ (BJD-2457000) | $1604.02376^{+0.00033}_{-0.00032}$ | $1602.50256^{+0.00091}_{-0.00093}$ |
| $P$ (days) | $6.9594731 \pm 2.2 \times 10^{-6}$ | $14.334892 \pm 1.2 \times 10^{-5}$ |
| $R_P/R_\star$ | $0.0664^{+0.0015}_{-0.0014}$ | $0.0528^{+0.0023}_{-0.0024}$ |
| $b$ | $0.03^{+0.19}_{-0.22}$ | $0.26^{+0.20}_{-0.58}$ |
| $\sqrt{e}\sin\omega$ | $-0.06^{+0.097}_{-0.081}$ | $-0.02^{+0.13}_{-0.11}$ |
| $\sqrt{e}\cos\omega$ | $-0.07^{+0.32}_{-0.39}$ | $-0.01^{+0.39}_{-0.38}$ |
| | Derived Parameters | |
| $a/R_\star$ | $11.66^{+0.24}_{-0.27}$ | $19.14^{+0.63}_{-0.81}$ |
| $i$ (°) | $89.88^{+1.08}_{-0.93}$ | $89.2^{+1.75}_{-0.64}$ |
| $T_{14}$ (days) | $0.202^{+0.047}_{-0.015}$ | $0.236^{+0.039}_{-0.032}$ |
| $R_P$ ($R_J$) | $0.891^{+0.021}_{-0.02}$ | $0.708^{+0.031}_{-0.032}$ |
| $a$ (AU) | $0.0748^{+0.0016}_{-0.0018}$ | $0.1228^{+0.0042}_{-0.0053}$ |
| $T_{\rm eq}$ (K)[a] | $1175.0^{+13.0}_{-12.0}$ | $917.0^{+19.0}_{-15.0}$ |
| $e$ | $0.064^{+0.187}_{-0.049}$ | $0.077^{+0.195}_{-0.056}$ |
| $\omega$ (°) | $195.3^{+140.0}_{-50.0}$ | $186.6^{+160.0}_{-140.0}$ |

**Note.**
[a] Assuming zero albedo.

fractional uncertainty on the model added in quadrature with the reported uncertainties.

For the transit model, we fit for $R_p/R_*$, $T_0$, semimajor axis-to-star radius ratio ($a/R_*$), orbital inclination ($i$), and two quadratic limb-darkening coefficients ($u_1$, $u_2$). For simplicity, we fixed the eccentricity ($e$) to zero. We put a Gaussian prior on the parameters $a/R_*$ and $i$ using the result of the TESS fit (Table 1) and on $u_1$ and $u_2$ using the `LDTK` toolkit (H. Parviainen & S. Aigrain 2015). The remaining parameters, $T_0$ and $R_p/R_*$, were allowed to vary within their physically plausible ranges (e.g., $T_0 > 0$ and $0 < R_p/R_* < 1$).

For each fit, we used 100 walkers for 100,000 steps and a 15,000-step burn in. We fit each of the four bands of the MuSCAT4 data separately, as well as a separate fit to the combined Sinistro $r'$ light curve.

As a test, we modeled the transits with a `BATMAN` model, and a GP as was done for the TESS data. We found the fits agreed within uncertainties. Similarly, we tried fitting the transits with the `BATMAN` model and a second-order polynomial but opting to mask the spot-crossing perturbations instead of explicitly modeling them as Gaussians. Again, all depths agreed within uncertainties. That is, our approach to fitting the data did not change any conclusions with respect to the chomaticity of the transit depth.

We show each transit fit and residuals as well as the transit depth posteriors in Figure 3. We list the best-fit parameters for each transit in Table 2. The depths in each wavelength agreed with each other to $<2\sigma$.

## 7. False-positive Analysis

For an initial assessment, we use `TRICERATOPS` (S. Giacalone & C. D. Dressing 2020; S. Giacalone et al. 2021), which calculates the probabilities of various transit-like scenarios in a Bayesian framework. Based on the flattened (GP removed) TESS light curves, `TRICERATOPS` estimated a false-positive probability of $<10^{-6}$.

While this appears to validate the planet, a statistical false-positive assessment using the light-curve morphology, as with `TRICERATOPS`, may be complicated by spot crossings and the need to flatten the data. However, an abundance of other evidence strongly indicates HIP 67522c is real:

1. Multitransiting systems have lower intrinsic (prior) probabilities of being false positives (J. J. Lissauer et al. 2012; J. F. Rowe et al. 2014; H. Valizadegan et al. 2023).
2. The spot crossings indicate the transiting/eclipsing body is passing in front of an active star. This favors HIP 67522, as an unassociated background/foreground star is unlikely to be so active.
3. The follow-up imaging, velocities, and color–magnitude diagram position from A. C. Rizzuto et al. (2020) already rule out any eclipsing binary or background star. The overwhelming majority of bound companions bright enough to reproduce the c transit would similarly have been detected in the existing follow-up (M. L. Wood et al. 2021).
4. The transit depths are consistent across three instruments spanning more than five years and wavelengths from Sloan Digital Sky Survey (SDSS) $g'$ to $z_s$. This consistency rules out any realistic stellar or instrumental signal.
5. The lack of chromaticity sets tight limits on the color of the source of the transit (J.-M. Désert et al. 2015). Following B. M. Tofflemire et al. (2021), we set a limit of $g' - z_s < 2.25$ for the host star. A bound companion within this limit will be $\simeq$20% as bright as the primary in the optical (A. Bressan et al. 2012). Such a target would be detected in existing high-SNR spectra and imaging (M. L. Wood et al. 2021) and show as an elevated color–magnitude diagram position (A. C. Rizzuto et al. 2017).
6. Following A. Vanderburg et al. (2019), the transit shape and depth sets the faintest companion, which could cause the transit signals to be $\Delta T < 1.5$ mags. As with the color constraints, such a star would be detected in one of the suite of follow-up given in A. C. Rizzuto et al. (2017) or M. L. Wood et al. (2021).
7. The detection of TTVs in HIP 67522b *predicted* the presence of HIP 67522c near an integer period ratio. The probability of any false-positive landing near a period ratio by chance is small and would not explain the TTV seen in HIP 67522b.

We conclude that the signal from HIP 67522c is unambiguously a real planet.

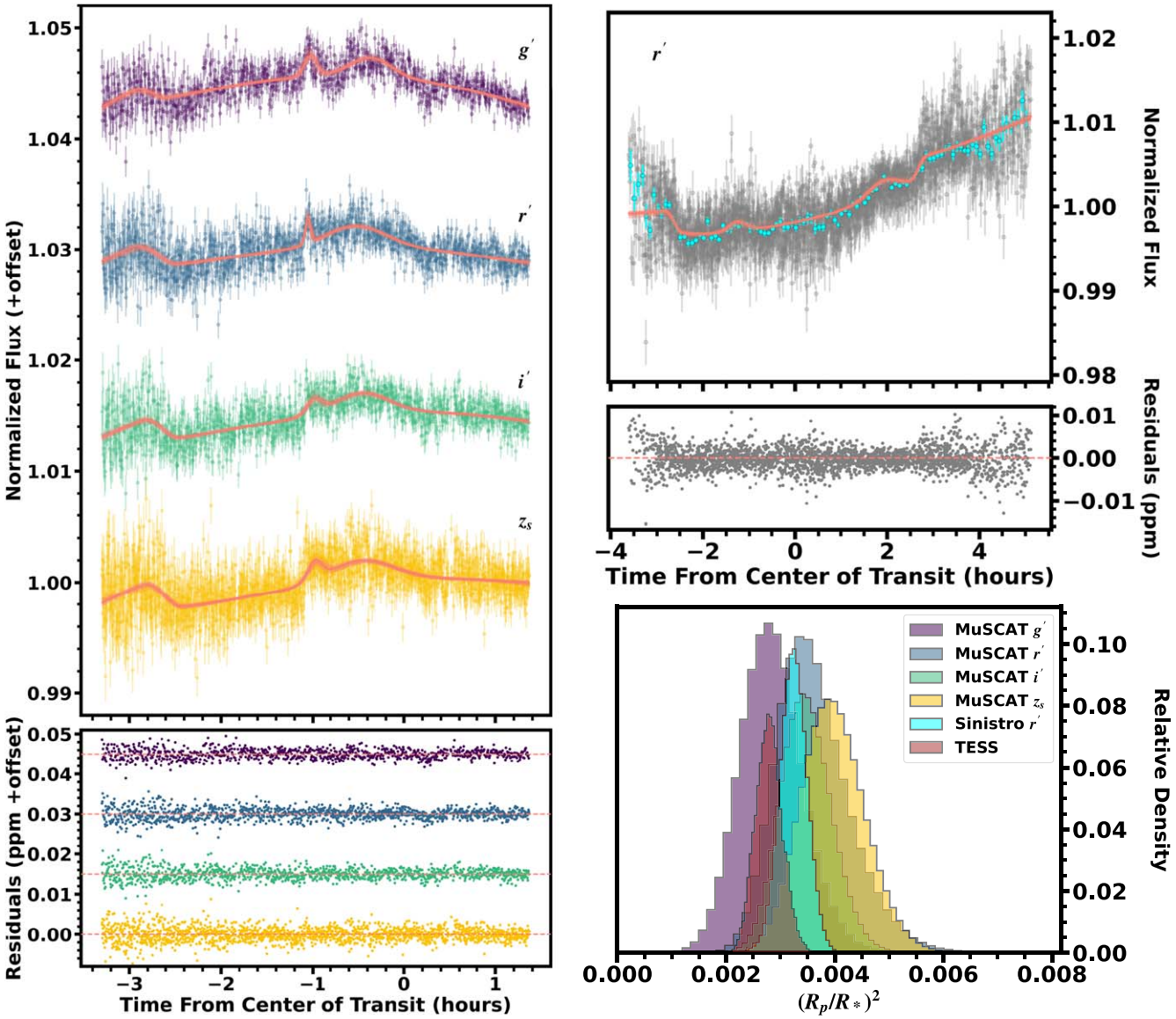


**Figure 3.** Ground-based follow-up transits of HIP 67522c from MuSCAT4 (left) and Sinistro (top right), with 5 minute bins shown for clarity. The MuSCAT4 transits were taken simultaneously, with each filter fitted separately. The three simultaneous Sinistro $r'$ transits were stacked and fit together. Each filter was fit with a `BATMAN` model, two Gaussian spot models, and a second-order polynomial to account for stellar variability. The opaque pink lines are the best-fit model, and the translucent lines are 100 models pulled from the fit posterior. The residuals for each transit are also shown. Bottom right: transit depth, measured by $(R_p/R_*)^2$, posterior from each of the transit fits. The data sets used to create this figure are available for download from the online journal.

(The data used to create this figure are available in the online article.)

## 8. Summary and Conclusions

We report the discovery and validation of HIP 67522c, originally identified as a single-transit event by A. C. Rizzuto et al. (2020). We find HIP 67522c to be $0.71 R_J$ ($7.9\ R_\oplus$) and near the 2:1 MMR with HIP 67522b. We confirm the period and transit depth with two follow-up ground-based transit observations taken with MuSCAT4 and Sinistro. The HIP 67522 system is now the youngest-known transiting multiplanet system to date.

The TESS fit posterior of planet b and c is suggestive of low-eccentricity orbits ($<0.36$ and $<0.39$ at 95% confidence, respectively); the maximum likelihood solution yields an eccentricity of 0.007 for planet b and 0.004 for planet c, with most of the high-eccentricity tail corresponding to specific values of $\omega$ where $e$ variations have low impact on the transit duration. The single-transit fit by A. C. Rizzuto et al. (2020) found HIP 67522c favored a higher eccentricity ($0.29 \pm 0.15$), but this assumed a planetary period $>24$ days.

Many of the young transiting multiplanet systems are also near MMR (e.g., AU Mic b and c (9:4) (P. Plavchan et al. 2020; E. Martioli et al. 2021), V1289 Tau c and d (3:2) and d and b (2:1) (T. J. David et al. 2019a, 2019b; A. D. Feinstein et al. 2022), HD 109833 b and c (3:2) (M. L. Wood et al. 2023), and TIC 434398831 b and c (5:3) (S. Vach et al. 2024a, 2024b)). Simulations suggest that planets will form in MMR and will begin to drift once the disk dissipates (~5 Myr; A. Izidoro et al. 2017), although many mature planets are found at or near MMR (e.g., J. H. Steffen & J. A. Hwang 2015). J. H. Hamer & K. C. Schlaufman (2024) suggest that MMRs should be most common in systems from 10 to 100 Myr, and F. Dai et al. (2024) note that such an excess is visible in the known population of young planets.

**Table 2**
Ground-based Transit Fits Using Gaussian Spot Models, a Second-order Polynomial, and Transit Model

| Parameter | MuSCAT $g'$ | MuSCAT $r'$ | MuSCAT $i'$ | MuSCAT $z_s$ | Sinistro $r'$ |
|---|---|---|---|---|---|
| | | | Transit Parameters | | |
| $t_{0,O} - t_{0,C}$ (days) | $-0.0049^{+0.0075}_{-0.0098}$ | $-0.0078^{+0.011}_{-0.014}$ | $0.0028^{+0.0074}_{-0.0062}$ | $0.0039^{+0.0076}_{-0.0064}$ | $0.00096^{+0.00087}_{-0.00086}$ |
| $R_p/R_*$ | $0.0531^{+0.0053}_{-0.0054}$ | $0.0595^{+0.0058}_{-0.0050}$ | $0.0588 \pm 0.0039$ | $0.0629 \pm 0.0046$ | $0.0569^{+0.0023}_{-0.0021}$ |
| $a/R_*$ | $19.24 \pm 0.74$ | $19.35 \pm 0.75$ | $19.21 \pm 0.73$ | $19.13 \pm 0.73$ | $19.62^{+0.65}_{-0.58}$ |
| $i$ (°) | $89.00^{+0.53}_{-0.51}$ | $88.69^{+0.66}_{-0.47}$ | $89.19 \pm 0.45$ | $89.18^{+0.47}_{-0.46}$ | $89.12^{+0.30}_{-0.36}$ |
| $u_1$ | $0.667 \pm 0.074$ | $0.471^{+0.075}_{-0.076}$ | $0.378^{+0.074}_{-0.073}$ | $0.370^{+0.076}_{-0.075}$ | $0.321^{+0.070}_{-0.071}$ |
| $u_2$ | $0.047 \pm 0.040$ | $0.129^{+0.039}_{-0.040}$ | $0.14 \pm 0.04$ | $0.159^{+0.040}_{-0.039}$ | $0.11 \pm 0.04$ |
| | | | Stellar Variability Parameters | | |
| $a$ | $0.99779 \pm 0.00019$ | $0.99890 \pm 0.00020$ | $0.99803 \pm 0.00018$ | $0.99818^{+0.00022}_{-0.00021}$ | $0.99908^{+0.00024}_{-0.00025}$ |
| $b$ | $0.112^{+0.014}_{-0.013}$ | $0.088^{+0.017}_{-0.014}$ | $0.092^{+0.011}_{-0.012}$ | $0.090 \pm 0.015$ | $0.0084^{+0.0046}_{-0.0042}$ |
| $c$ | $-0.493^{+0.053}_{-0.059}$ | $-0.36^{+0.06}_{-0.08}$ | $-0.334^{+0.046}_{-0.044}$ | $-0.299^{+0.060}_{-0.058}$ | $0.064^{+0.012}_{-0.013}$ |
| | | | Spot Parameters | | |
| $A_1$ | $0.00194^{+0.00034}_{-0.00030}$ | $0.00225^{+0.00046}_{-0.00047}$ | $0.00136^{+0.00027}_{-0.00026}$ | $0.00170 \pm 0.00028$ | $0.00112^{+0.00027}_{-0.00029}$ |
| $\tau_1$ (days) | $0.00289^{+0.00056}_{-0.00062}$ | $0.00121^{+0.00038}_{-0.00026}$ | $0.00356^{+0.00072}_{-0.00081}$ | $0.00377^{+0.00071}_{-0.00083}$ | $0.0085^{+0.0017}_{-0.0029}$ |
| $t_{sp1}$ (BJD-2457000) | $3422.99112 \pm 0.00061$ | $3422.98998^{+0.00033}_{-0.00028}$ | $3422.99308 \pm 0.00094$ | $3422.99358^{+0.00084}_{-0.00092}$ | $3437.3172^{+0.0024}_{-0.0033}$ |
| $A_2$ | $0.00167 \pm 0.00018$ | $0.00191 \pm 0.00017$ | $0.00179 \pm 0.00016$ | $0.00193^{+0.00018}_{-0.00019}$ | $0.00193^{+0.00023}_{-0.00025}$ |
| $\tau_2$ (days) | $0.00932^{+0.00091}_{-0.00083}$ | $0.0138^{+0.0015}_{-0.0013}$ | $0.0119^{+0.0012}_{-0.0013}$ | $0.0142^{+0.0016}_{-0.0019}$ | $0.0142^{+0.0026}_{-0.0033}$ |
| $t_{sp2}$ (BJD-2457000) | $3423.0187 \pm 0.0010$ | $3423.0119 \pm 0.0012$ | $3423.0147 \pm 0.0013$ | $3423.015 \pm 0.0015$ | $3437.4488^{+0.0018}_{-0.0019}$ |
| $\ln f$ | $-7.382^{+0.080}_{-0.089}$ | $-7.55^{+0.10}_{-0.12}$ | $-7.59^{+0.14}_{-0.11}$ | $-7.40^{+0.14}_{-0.11}$ | $-6.513^{+0.033}_{-0.032}$ |

The transit depth is consistent across wavelengths from SDSS $g'$ to $z_s$ to within $2\sigma$, but it is interesting to note the transit depth trends deeper with increasing wavelength. Aside from a statistical coincidence, it may be a bias from the spot crossing and/or additional undetected (and hence not modeled) spot crossings. Alternatively, this may be due to an unocculted hot spot, which will make blue transits appear shallower (e.g.,; B. V. Rackham et al. 2018).

Our ground-based transits and many of the TESS transits show evidence of spot crossings or local flares, far more than is seen in transits of HIP 67522b in the TESS data. This suggests that HIP 67522c crosses a more active latitude of the host star. It may be possible to take advantage of the spot occultations in the TESS transits to derive planetary and spot characteristics (e.g., B. M. Morris et al. 2017) and the stellar obliquity (J.-M. Désert et al. 2011). Simultaneous multiband photometry, in particular, can be used to better characterize spot coverage and temperature (M. Mori et al. 2024).

Unfortunately, our single multiband transit provides only weak constraints on the spot properties. For the second spot, the amplitude is relatively flat with wavelength, which is more consistent with cool (<4500 K) spots. Although the relatively large uncertainties make it challenging to break the degeneracy between spot size and temperature.

HIP 67522b was a Cycle 1 JWST target (A. W. Mann et al. 2021). The resulting transmission spectrum showed strong features, with the transit depth varying by ≃50% in the $CO_2$ and $H_2O$ bands, consistent with a low-density planet (P. C. Thao et al. 2024, in preparation). HIP 67522c is only ≃20% smaller than HIP 67522b ($0.71R_J$ versus $0.89R_J$). Assuming it also has a low density, as predicted for such young planets (J. E. Owen 2020), it will be a similarly high-priority target for JWST.

## Acknowledgments

The authors wish to thank Halee, Wally, Penny, and Bandit for their invaluable support. M. G. B. was supported by the NSF Graduate Research Fellowship (DGE-2040435), the NC Space Grant Graduate Research Fellowship, and the TESS Guest Investigator Cycle 5 program (21-TESS21-0016; NASA Grant number 80NSSC24K0880). P. C. T. was supported by the NSF Graduate Research Fellowship (DGE-1650116), the Jack Kent Cooke Foundation Graduate Scholarship, and the JWST GO program (2498). A. W. M. was supported by the NSF CAREER program (AST-2143763) and a grant from NASA's Exoplanet Research Program (XRP 80NSSC21K0393). This work is partly supported by JSPS KAKENHI grant No. JPJP24H00017 and JSPS Bilateral Program No. JPJSBP120249910.

This Letter makes use of data collected by the TESS mission. Funding for the TESS mission is provided by NASAs Science Mission Directorate. We acknowledge the use of public TESS data from pipelines at the TESS Science Office and at the TESS Science Processing Operations Center. Resources supporting this work were provided by the NASA High-End Computing (HEC) Program through the NASA Advanced Supercomputing (NAS) Division at Ames Research Center for the production of the SPOC data products. TESS data presented in this Letter were obtained from the Mikulski Archive for Space Telescopes (MAST) at the Space Telescope Science Institute (STScI).

This work makes use of observations from the Las Cumbres Observatory Global Telescope Network. Some data in the Letter are based on observations made with the MuSCAT3/4 instruments, developed by the Astrobiology Center (ABC) in Japan, the University of Tokyo, and Las Cumbres Observatory (LCOGT). MuSCAT3 was developed with financial support by JSPS KAKENHI (JP18H05439) and JST PRESTO (JPMJPR1775) and is located at the Faulkes Telescope North on Maui, HI (USA), operated by LCOGT. MuSCAT4 was developed with financial

support provided by the Heising-Simons Foundation (grant 2022-3611), JST grant number JPMJCR1761, and the ABC in Japan and is located at the Faulkes Telescope South at Siding Spring Observatory (Australia), operated by LCOGT.

*Facilities:* TESS, LCOGT.

*Software:* `MISTTBORN`, `astropy` (Astropy Collaboration et al. 2013, 2018, 2022), `Notch & LoCoR`, `TRICERATOPS`.

## ORCID iDs

Madyson G. Barber https://orcid.org/0000-0002-8399-472X
Pa Chia Thao https://orcid.org/0000-0001-5729-6576
Andrew W. Mann https://orcid.org/0000-0003-3654-1602
Andrew Vanderburg https://orcid.org/0000-0001-7246-5438
Mayuko Mori https://orcid.org/0000-0003-1368-6593
John H. Livingston https://orcid.org/0000-0002-4881-3620
Akihiko Fukui https://orcid.org/0000-0002-4909-5763
Norio Narita https://orcid.org/0000-0001-8511-2981
Adam L. Kraus https://orcid.org/0000-0001-9811-568X
Benjamin M. Tofflemire https://orcid.org/0000-0003-2053-0749
Elisabeth R. Newton https://orcid.org/0000-0003-4150-841X
Joshua N. Winn https://orcid.org/0000-0002-4265-047X
Jon M. Jenkins https://orcid.org/0000-0002-4715-9460
Sara Seager https://orcid.org/0000-0002-6892-6948
Karen A. Collins https://orcid.org/0000-0001-6588-9574
Joseph D. Twicken https://orcid.org/0000-0002-6778-7552

## References

Astropy Collaboration, Price-Whelan, A. M., Lim, P. L., et al. 2022, ApJ, 935, 167
Astropy Collaboration, Price-Whelan, A. M., Sipőcz, B. M., et al. 2018, AJ, 156, 123
Astropy Collaboration, Robitaille, T. P., Tollerud, E. J., et al. 2013, A&A, 558, A33
Baraffe, I., Homeier, D., Allard, F., & Chabrier, G. 2015, A&A, 577, A42
Barat, S., Désert, J.-M., Goyal, J. M., et al. 2024, arXiv:2407.14995
Bressan, A., Marigo, P., Girardi, L., et al. 2012, MNRAS, 427, 127
Capistrant, B. K., Soares-Furtado, M., Vanderburg, A., et al. 2024, AJ, 167, 54
Dai, F., Goldberg, M., Batygin, K., et al. 2024, arXiv:2406.06885
Dai, F., Winn, J. N., Yu, L., & Albrecht, S. 2017, AJ, 153, 40
David, T. J., Cody, A. M., Hedges, C. L., et al. 2019b, AJ, 158, 79
David, T. J., Petigura, E. A., Luger, R., et al. 2019a, ApJL, 885, L12
Dawson, R. I., & Johnson, J. A. 2012, ApJ, 756, 122
Désert, J.-M., Charbonneau, D., Demory, B.-O., et al. 2011, ApJS, 197, 14
Désert, J.-M., Charbonneau, D., Torres, G., et al. 2015, ApJ, 804, 59
Feinstein, A. D., David, T. J., Montet, B. T., et al. 2022, ApJL, 925, l2
Fernandes, R. B., Hardegree-Ullman, K. K., Pascucci, I., et al. 2023, AJ, 166, 175
Fernandes, R. B., Mulders, G. D., Pascucci, I., et al. 2022, AJ, 164, 78
Foreman-Mackey, D. 2018, RNAAS, 2, 31
Foreman-Mackey, D., Agol, E., Ambikasaran, S., & Angus, R. 2017, AJ, 154, 220
Foreman-Mackey, D., Hogg, D. W., Lang, D., & Goodman, J. 2013, PASP, 125, 306
Fukui, A., Narita, N., Tristram, P. J., et al. 2011, PASJ, 63, 287
Gaia Collaboration, Vallenari, A., Brown, A. G. A., et al. 2023, A&A, 674, A1
Giacalone, S., & Dressing, C. D. 2020, Astrophysics Source Code Library, ascl:2002.004
Giacalone, S., Dressing, C. D., Jensen, E. L. N., et al. 2021, AJ, 161, 24
Gilbert, E. A., Barclay, T., Quintana, E. V., et al. 2022, AJ, 163, 147
Hamer, J. H., & Schlaufman, K. C. 2024, AJ, 167, 55
Heitzmann, A., Zhou, G., Quinn, S. N., et al. 2021, ApJL, 922, L1
Hirano, T., Gaidos, E., Harakawa, H., et al. 2024, MNRAS, 530, 3117
Hirano, T., Krishnamurthy, V., Gaidos, E., et al. 2020, ApJL, 899, L13
Howell, S. B., Sobeck, C., Haas, M., et al. 2014, PASP, 126, 398
Izidoro, A., Ogihara, M., Raymond, S. N., et al. 2017, MNRAS, 470, 1750
Jenkins, J. M., Tenenbaum, P., Seader, S., et al. 2020, in Kepler Data Processing Handbook: Transiting Planet Search, Kepler Science Document KSCI-19081-003, ed. J. M. Jenkins
Jenkins, J. M., Twicken, J. D., McCauliff, S., et al. 2016, Proc. SPIE, 9913, 99133E
Johnson, M. C., Dai, F., Justesen, A. B., et al. 2018, MNRAS, 481, 596
Johnson, M. C., David, T. J., Petigura, E. A., et al. 2022, AJ, 163, 247
Kerr, R., Rizzuto, A. C., Kraus, A. L., et al. 2021, ApJ, 917, 23
Kipping, D. M. 2013, MNRAS, 435, 2152
Kreidberg, L. 2015, PASP, 127, 1161
Lammers, C., Hadden, S., & Murray, N. 2023, MNRAS, 525, L66
Lightkurve Collaboration, Cardoso, J. V. d. M., Hedges, C., et al. 2018, ascl:1812.013
Lissauer, J. J., Marcy, G. W., Rowe, J. F., et al. 2012, ApJ, 750, 112
Lissauer, J. J., Ragozzine, D., Fabrycky, D. C., et al. 2011, ApJS, 197, 8
Livingston, J. H., Dai, F., Hirano, T., et al. 2018, AJ, 155, 115
Mann, A. W., Gaidos, E., Mace, G. N., et al. 2016, ApJ, 818, 46
Mann, A. W., Gao, P., Kraus, A. L., et al. 2021, The Atmosphere of a 17 Myr Old Hot Jupiter, JWST Proposal. Cycle 1, ID #2498
Mann, A. W., Wood, M. L., Schmidt, S. P., et al. 2022, AJ, 163, 156
Martioli, E., Hébrard, G., Correia, A. C. M., Laskar, J., & Lecavelier des Etangs, A. 2021, A&A, 649, A177
Masuda, K. 2014, ApJ, 783, 53
McCully, C., Volgenau, N. H., Harbeck, D.-R., et al. 2018, Proc. SPIE, 10707, 107070K
Mori, M., Ikuta, K., Fukui, A., et al. 2024, MNRAS, 530, 167
Morris, B. M., Hebb, L., Davenport, J. R. A., Rohn, G., & Hawley, S. L. 2017, ApJ, 846, 99
Morris, R. L., Twicken, J. D., Smith, J. C., et al. 2020, in Kepler Data Processing Handbook: Photometric Analysis, Kepler Science Document KSCI-19081-003, ed. J. M. Jenkins (Kepler Science Document KSCI-19081-003)
Nardiello, D., Malavolta, L., Desidera, S., et al. 2022, A&A, 664, A163
Narita, N., Fukui, A., Yamamuro, T., et al. 2020, Proc. SPIE, 11447, 114475K
Owen, J. E. 2020, MNRAS, 498, 5030
Parviainen, H., & Aigrain, S. 2015, MNRAS, 453, 3821
Plavchan, P., Barclay, T., Gagné, J., et al. 2020, Natur, 582, 497
Rackham, B. V., Apai, D., & Giampapa, M. S. 2018, ApJ, 853, 122
Ratzenböck, S., Großschedl, J. E., Möller, T., et al. 2023, A&A, 677, A59
Ricker, G. R., Winn, J. N., Vanderspek, R., et al. 2015, JATIS, 1, 014003
Rizzuto, A. C., Mann, A. W., Vanderburg, A., Kraus, A. L., & Covey, K. R. 2017, AJ, 154, 224
Rizzuto, A. C., Newton, E. R., Mann, A. W., et al. 2020, AJ, 160, 33
Rowe, J. F., Bryson, S. T., Marcy, G. W., et al. 2014, ApJ, 784, 45
Smith, J. C., Stumpe, M. C., Van Cleve, J. E., et al. 2012, PASP, 124, 1000
Soderblom, D. R., Hillenbrand, L. A., Jeffries, R. D., Mamajek, E. E., & Naylor, T. 2014, in Protostars and Planets VI, ed. H. Beuther et al. (Tucson, AZ: Univ. of Arizona Press), 219
Steffen, J. H., Fabrycky, D. C., Ford, E. B., et al. 2012, MNRAS, 421, 2342
Steffen, J. H., & Hwang, J. A. 2015, MNRAS, 448, 1956
Stumpe, M. C., Smith, J. C., Catanzarite, J. H., et al. 2014, PASP, 126, 100
Stumpe, M. C., Smith, J. C., Van Cleve, J. E., et al. 2012, PASP, 124, 985
Thao, P. C., Mann, A. W., Barber, M. G., et al. 2024, AJ, 168, 41
Tofflemire, B. M., Rizzuto, A. C., Newton, E. R., et al. 2021, AJ, 161, 171
Twicken, J. D., Clarke, B. D., Bryson, S. T., et al. 2010, Proc. SPIE, 7740, 774023
Vach, S., Zhou, G., Huang, C. X., et al. 2024a, AJ, 167, 210
Vach, S., Zhou, G., Huang, C. X., et al. 2024b, arXiv:2407.19680
Valizadegan, H., Martinho, M. J. S., Jenkins, J. M., et al. 2023, AJ, 166, 28
Van Eylen, V., & Albrecht, S. 2015, ApJ, 808, 126
Vanderburg, A., Huang, C. X., Rodriguez, J. E., et al. 2019, ApJL, 881, L19
Wood, M. L., Mann, A. W., Barber, M. G., et al. 2023, AJ, 165, 85
Wood, M. L., Mann, A. W., & Kraus, A. L. 2021, AJ, 162, 128
Zakhozhay, O. V., Launhardt, R., Trifonov, T., et al. 2022, A&A, 667, L14